Estimating the hydraulic properties of the fracture network in a sandstone aquifer

Hitchmough, A; Herbert, AW; Riley, Michael; Tellam, John

DOI:
10.1016/j.jconhyd.2007.01.012

Document Version
Publisher's PDF, also known as Version of record

Citation for published version (Harvard):
Hitchmough, A, Herbert, AW, Riley, M & Tellam, J 2007, 'Estimating the hydraulic properties of the fracture network in a sandstone aquifer', *Journal of Contaminant Hydrology*, vol. 93, pp. 38-57.
https://doi.org/10.1016/j.jconhyd.2007.01.012

Available online at www.sciencedirect.com
ScienceDirect
Journal of Contaminant Hydrology 93 (2007) 38–57
JOURNAL OF Contaminant Hydrology
www.elsevier.com/locate/jconhyd

Estimating the hydraulic properties of the fracture network in a sandstone aquifer

Anna M. Hitchmough [1], Michael S. Riley, Alan W. Herbert [2], John H. Tellam *

Hydrogeology Research Group, Earth Sciences, School of Geography, Earth and Environmental Sciences, University of Birmingham, Edgbaston, Birmingham B15 2TT, UK

Received 17 January 2006; received in revised form 12 January 2007; accepted 15 January 2007
Available online 26 January 2007

Abstract

The potential hydraulic behaviour of the fracture network in a major Triassic sandstone aquifer in the UK has been evaluated. The properties of the fracture network were determined using results from detailed scan line surveys at 10 sites, television and geophysical borehole logging, and packer testing. Six sets of discontinuities common to all sites were identified and statistically characterised (dip, strike, orientation, density, size, and estimated transmissivity). A discrete fracture network model was then used stochastically to investigate the properties of the network. In general, the network is poorly connected: it is estimated that 9% of the discontinuities intersecting boreholes are transmissive. The hydraulic behaviour of the network is generally dominated by one sub-horizontal bedding plane fracture set, although when present, a relatively infrequent north–south striking, sub-vertical set modifies the bulk flow properties significantly. Ignoring this latter set, the network's minimum representative volume is about $35 \times 35 \times 35$ m. The upscaled permeability is anisotropic, being typically 23 times greater in the horizontal than in the vertical. Tortuosity in the north–south direction is around 1.6.

Keywords: Sandstone; Fractured rock; Effective permeability; Tortuosity

1. Introduction

Apart from the occasional generic investigation using numerical models (e.g. Odling and Roden, 1997; Manzochi et al., 1998), there are few quantitative descriptions of flow through fractured, permeable matrix aquifers (National Research Council, 2001; Dietrich et al., 2005). This paper describes a preliminary stage in the development of a quantitative description of flow through the UK Triassic Sandstone, a fractured, permeable matrix red bed sequence. Only the properties of the fracture network are considered. Data on the discontinuity properties have been collected from one of the main UK Permo–Triassic Sandstone basins: hydraulic information was obtained from packer test data, and geometric and frequency information from scan line surveys and borehole logs. The fracture network has been partitioned into sets and statistically characterised by inferring distributions of transmissivity, dip, strike, density and size, and its description employed in a stochastic analysis of the hydraulic properties of the network using a discrete

* Corresponding author. Tel.: +44 121 414 6138; fax: +44 121 414 4942.
E-mail address: J.H.Tellam@bham.ac.uk (J.H. Tellam).
[1] Now of Bureau Veritas, Blakelands House, 400 Aldridge Road, Birmingham, B44 8BH, UK.
[2] Now of ESI Ltd, New Zealand House, 160 Abbey Foregate, Shrewsbury, SY2 6BZ, UK.

0169-7722/$ - see front matter © 2007 Elsevier B.V. All rights reserved.
doi:10.1016/j.jconhyd.2007.01.012

fracture network flow code. Finally, the implications of the numerical investigation have been assessed.

2. The UK Permo–Triassic Sandstone

The UK Permo–Triassic Sandstone is a fluviatile and aeolian red bed sequence with typical matrix intergranular permeability and porosity of 0.1–10 md^{-1} and 0.15–0.30 respectively (e.g. Allen et al., 1997). Bed thickness ranges up to 3 m or more, but is often less than 1 m. Cross-lamination and cross-bedding are common. Shear strength is typically low, ranging between overconsolidated sand to weak rock (Yates, 1992; Hawkins and McConnell, 1992). A comprehensive description of the sequence is given by Benton et al. (2002), and aspects of flow and solute transport covered by Barker and Tellam (2006). Fracturing comprises bedding plane joints, non-bedding plane joints, and faults (Allen et al., 1998); granulation seams (millimetre thick cataclastites of very low porosity) are also quite common (Fowles and Burley, 1994). Below, the term "discontinuities" will be used to include both fractures (of whatever origin) and granulation seams: the term "fractures" will exclude granulation seams but include all other discontinuities.

There is considerable evidence that fracturing affects flow in the aquifer, but most of this evidence comes from studies of zones immediately around boreholes: due to drilling and pumping damage, flow in this zone may not be representative of flow remote from boreholes. Nevertheless, the evidence available includes: packer test data (Price, 1982; Walthall and Ingram, 1984; Brassington and Walthall, 1985); borehole logging and core data (Brereton and Skinner, 1974; Walters, 1985; Entec, 1997); intergranular/field test comparisons (Walthall and Campbell, 1986; Allen et al., 1997); and tracer test data (Barker et al., 1998; Streetly et al., 2002). Allen et al. (1998) and Tellam and Barker (2006) provide more detailed discussion of this evidence.

In summary, these data indicate that fractures are common near boreholes, that they can considerably affect the apparent transmissivity as measured using pumping methods, and that they appear to be less prevalent at depth. The only direct evidence of the importance of fractures to larger scale flow is a tracer test over about 280 m (Barker et al., 1998), which suggested an average linear velocity of 140 md^{-1}, a value at least two orders of magnitude higher than that suggested by regional gradients and intergranular permeability. Comparison of matrix permeability data with permeabilities estimated by regional groundwater flow modelling also suggests that fractures contribute to regional groundwater flow (Allen et al., 1997). In one regional flow modelling study it was found necessary to reduce bulk rock permeability below a depth of approximately 150–200 m in order to obtain an adequate representation of the flow system, and this was justified by the reduction in fracture frequency noted in closed circuit television (CCTV) logs (Allen, 1969; Campbell, 1982; Howard, 1988). There are few regional studies of fracturing in the sandstones. Plant et al. (1996), Chadwick (1997) and Knott (1994) describe faulting in the tectonic framework of the sandstone sequences in the Cheshire Basin and elsewhere in Northwest England. On the local scale, Wealthall et al. (2001) discuss the hydrogeological implications of large infilled fractures. Detailed studies have also been carried out by Barnes et al. (1998) and Gutmanis et al. (1998) in the Sellafield region of Northwest England in the context of radioactive waste disposal safety assessments.

3. Field data collection methods and computer code

3.1. Scan line discontinuity surveys

Scan line surveys were undertaken at 10 sites in the Cheshire Basin, England (Fig. 1, Table 1). At most sites, surveys were possible in more than one direction (Table 1). The procedure followed that of Anon (1997) and ISRM (1978). The parameters recorded and their definitions are given in Table 2.

As other workers have found (e.g. Robertson, 1970), scan line surveys do include significant subjectivity, and this is reflected in their relatively poor repeatability compared with many hydrogeological measurements. Consequently, a series of investigations was conducted to assess the quality of the survey data collected. This included tests on (i) repeatability of scan line results in which the same surveyor returned to the same scan line after intervals of time ranging between hours and months; and (ii) the robustness of the results from different individuals with varying experience surveying the same scan lines.

Fig. 2 shows the results of repeated surveys by the same, well-experienced surveyor. The agreement is good for 1999 and 2000. The 1997 survey used a horizontal scan line parallel to the two later surveys, but with an elevation 20 cm lower: although similar to the other surveys, it is clear that even a 20 cm displacement can made a recognisable difference to the survey results.

Following completion of data collection, a further site was chosen comprising three 5-metre scan lines that were surveyed independently by three individuals. In this test, the two less experienced surveyors, B and C, had not undertaken any surveying for several months. Fig. 3 gives illustrative data indicating that the two less

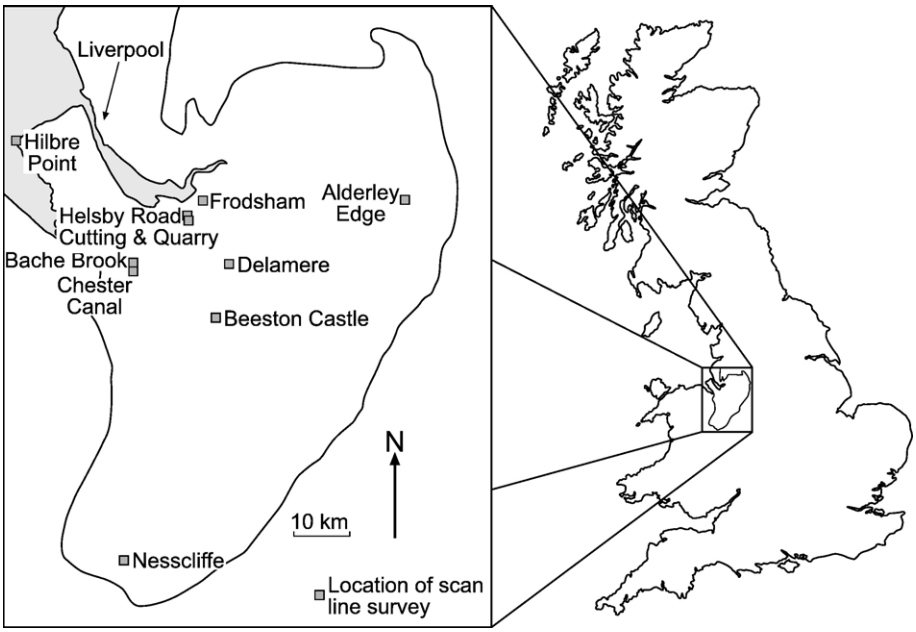

Fig. 1. The Cheshire Basin with locations of the scan line surveys.

experienced surveyors recorded only 60% and 74% of the discontinuities to within 10 cm of the location recorded by the experienced surveyor. All three surveyors identified the five longest discontinuity traces and recorded similar length distributions with average lengths of 2 m (most experienced surveyor), 2.1 m, and 1.8 m; median lengths of 1.5 m, 1.4 m, and 1.4 m; minimum lengths of 0.3 m, 0.2 m, and 0.2 m; and maximum lengths of 5 m, 5 m, and 8.5 m. Censoring and fill distributions were the least reproducible attributes.

In general, it was concluded that, provided the surveyors were experienced, the uncertainties due to incorrect measurements (compare Fig. 2 with Fig. 3) were smaller than those resulting from vertical changes of scan line location (Fig. 2). It is not possible to assign formal errors for the surveying given the data available, but the results of the repeat surveys have tempered the decisions made when interpreting the full data set.

3.2. Borehole logging

Borehole logging of uncased boreholes was used to provide most of the data on the properties of subhorizontal fractures as almost all outcrop surveys had to be undertaken along horizontal scan lines (Table 1). The logging also provided indications of the amount of flow occurring in each fracture.

Fluid electrical conductivity, fluid temperature, calliper, flow (heat pulse), natural gamma, and closed circuit television logs were completed at six sites in the Cheshire Basin using Robertson Geologging Portalog and Telespec CCTV systems. Data from a further five sites in the Cheshire Basin were obtained from previous studies by Birmingham University and the North West Water Authority, summarised in University of Birmingham and NWWA (1981). The sites were chosen to include all the formations in the Triassic Sherwood Sandstone Group sequence.

Comparison of previous CCTV log interpretations of fractures with the original CCTV log video records showed that the previous interpretations did not record all discontinuities seen in the borehole walls. As a result, modifications (described in Section 5.2.3) were made to previous CCTV interpretations. Comparison of CCTV and calliper logs showed poor agreement in locating fractures: in addition, repeatability for calliper logs was poor, suggesting that many of the fractures give rise to borehole wall irregularities which are close to the detection limit of the device (as also concluded by Merin, 1992). Accordingly, calliper data were disregarded. Repeat temperature conductivity logs showed that the locations of slope changes are reliably located in each log provided the borehole column is not significantly disturbed.

3.3. The discrete fracture network code (NAPSAC)

Much of the investigation of the implications of the field data set was carried out using the finite element, 3D, discrete fracture network code, NAPSAC (Herbert,

Table 1
Summary of scan line locations, strikes and dimensions (vertical scan lines and horizontal outcrops are indicated)

Site	National grid reference	Scan line strike (°)	Scan line length (m)	Height of outcrop (m)	Number of discontinuities at site
Chester Canal A	SJ 401666	261	5.2	2.9	9
Chester Canal B		153	20	6	18
Chester Canal C		261	19	6.5	17
Bache Brook A	SJ 401680	180	10.6	4	16
Bache Brook B		260	3.5	5	8
Bache Brook C		Cuts Bache B	2	Vertical line	109
Bache Brook D		235	7.7	6	10
Beeston Castle A	SJ 539590	95	6	5.8	17
Beeston Castle B		30	3.4	4	10
Beeston Castle C		324	9.5	7	18
Delamere A	SJ 561677	350	20	5	18
Delamere B		77	6.7	4	8
Delamere C		115	14.7	1.5	26
Delamere D		332	10	9.7	11
Delamere E		225	7.5	5	31
Delamere F		324	11	6	1
Delamere G		354	20	2	15
Frodsham A	SJ 516780	301	8	8	9
Frodsham B		290	6.8	6.8	10
Frodsham C		117	9.2	9.2	5
Frodsham D		84	3.9	3.9	6
Frodsham E		268	7.2	7.2	11
Helsby Road Cutting	SJ 490757	2	27	3.52	29
Helsby Quarry A	SJ 491749	250	13.9	4	49
Helsby Quarry B		188	7	5.5	25
Helsby Quarry C		326	7.8	2.5	11
Helsby Quarry D		204	13.2	3.5	26
Helsby Quarry E		354	11.2	4	14
Helsby Quarry F		300	6	3	4
Helsby Quarry G		126	6	3	13
Hilbre Point	SJ 180880	152	10	2.25	14
Nesscliffe A	SJ 385195	92	7.1	3.5	17
Nesscliffe B		1	3.51	10	4
Nesscliffe C		11	2.85	10	2
Nesscliffe D		13	2.7	10	6
Nesscliffe E		59	4.3	7.62	14
Nesscliffe F		34	4.7	13.72	15
Nesscliffe G		314	3.9	10	12
Nesscliffe H		166	20	33.53	33
Nesscliffe I		174	13.9	21.33	30
Nesscliffe J		351	20	12.19	46
Nesscliffe K		80	6.8	12.19	24
Nesscliffe L		40	18.6	15.24	33
Alderley Edge (T) A	SJ 856780	338	20	5	30
Alderley Edge (T) B		151	20	4.34	6
Alderley Edge (T) C		235	4.4	4.4	8
Alderley Edge (T) D		293	20	3.5	46
Alderley Edge (T) E		317	10	Horizontal	4
Alderley Edge (T) F		164	10	7	18
Alderley Edge (W) A	SJ 856780	136	12.3	11	19
Alderley Edge (W) B		93	8.2	6	3
Alderley Edge (W) C		165	28	Horizontal	12
Alderley Edge (W) D		54	8	Horizontal	5
Alderley Edge (W) E		338	16	2.5	12
Alderley Edge (W) F		169	20	5	12

The Alderley Edge data have been divided into two groups, one representing discontinuities in the Wilmslow Sandstone Formation (marked (W)), and one representing discontinuities in the Thursaston Member of the Helsby Sandstone Formation (T).

Table 2
Parameters recorded in scan line surveys

Parameter	Definitions/comments
Position (m)	Location of discontinuity from end of scan line
Orientation (°)	Dip and strike of discontinuity
Trace length (m)	Length of discontinuity in the exposure
J_a	Joint alteration parameter of Barton et al. (1974)
JRC	Joint roughness coefficient of Barton (1973)
J_r	Joint roughness parameter of Barton et al. (1974)
Aperture (mm)	Estimated
Waviness (m)	Amplitude and wave length
Censoring	Uncensored, one end censored, or both ends censored

1992; Hartley, 1998). The code considers fracture flow only. Input data comprise statistical distribution parameters for each fracture set for fracture length, width, dip, strike, and orientation within the fracture plane, and fracture transmissivity. NAPSAC generates points in space based on the fracture density distributions using a uniform Poisson process. Dip, strike, orientation, length, and transmissivity are then assigned to each fracture using the input distributions.

NAPSAC has an inbuilt method for estimating effective hydraulic conductivity for a given realisation of the network geometry and transmissivity distribution. For a block of fractured rock, a sequence of uniform head gradients is applied to the faces of the block and the discharge across each face calculated using the NAPSAC flow solver. The effective hydraulic conductivity tensor is chosen to minimise the expression:

$$\sum_{j=1}^{15}\sum_{i=1}^{6}\left(Q_{i,j}^{\text{calc}}-Q_{i,j}^{\text{estimated}}\right)^2$$

where the subscripts i and j refer to the applied head gradients and the faces of the block respectively; $Q_{i,j}^{\text{calc}}$ is the calculated discharge; and $Q_{i,j}^{\text{estimated}}$ is the discharge estimated using the head gradient and the effective hydraulic conductivity tensor. The direction of the head gradient is defined by a line joining the midpoint of a pair of opposite edges of a randomly orientated, regular 20-

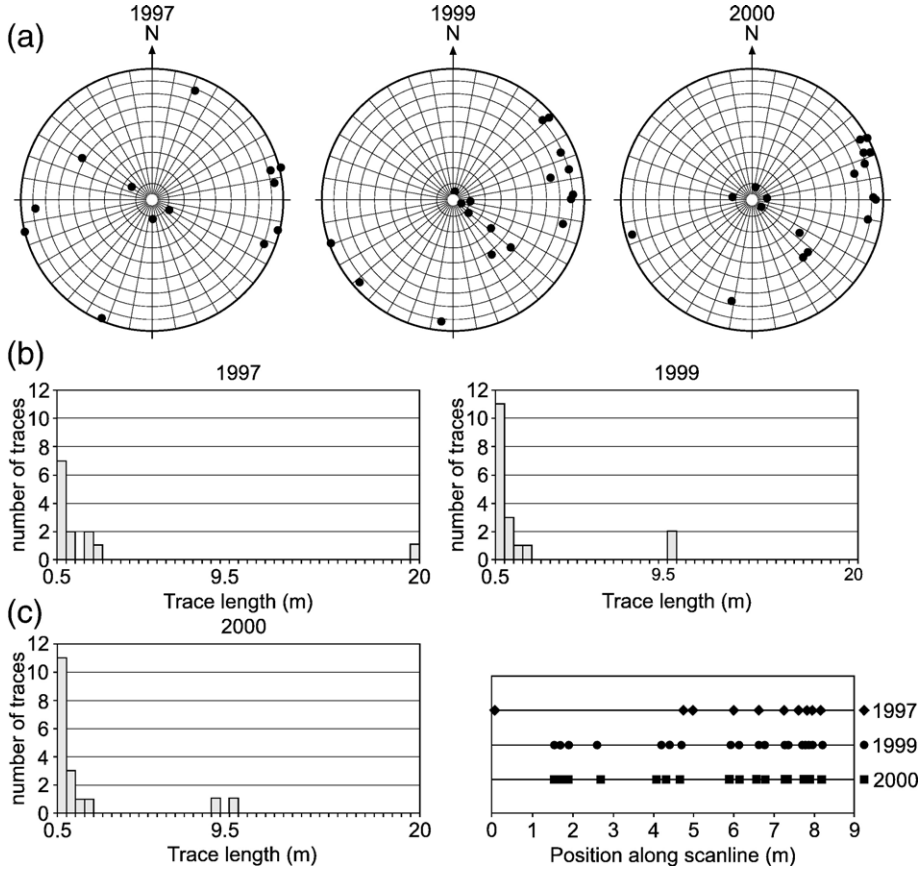

Fig. 2. Comparison of data measured in 1997, 1999, and 2000: (a) discontinuity orientations (upper hemisphere, equal area projection); (b) discontinuity trace lengths; (c) position of discontinuities along the scan line.

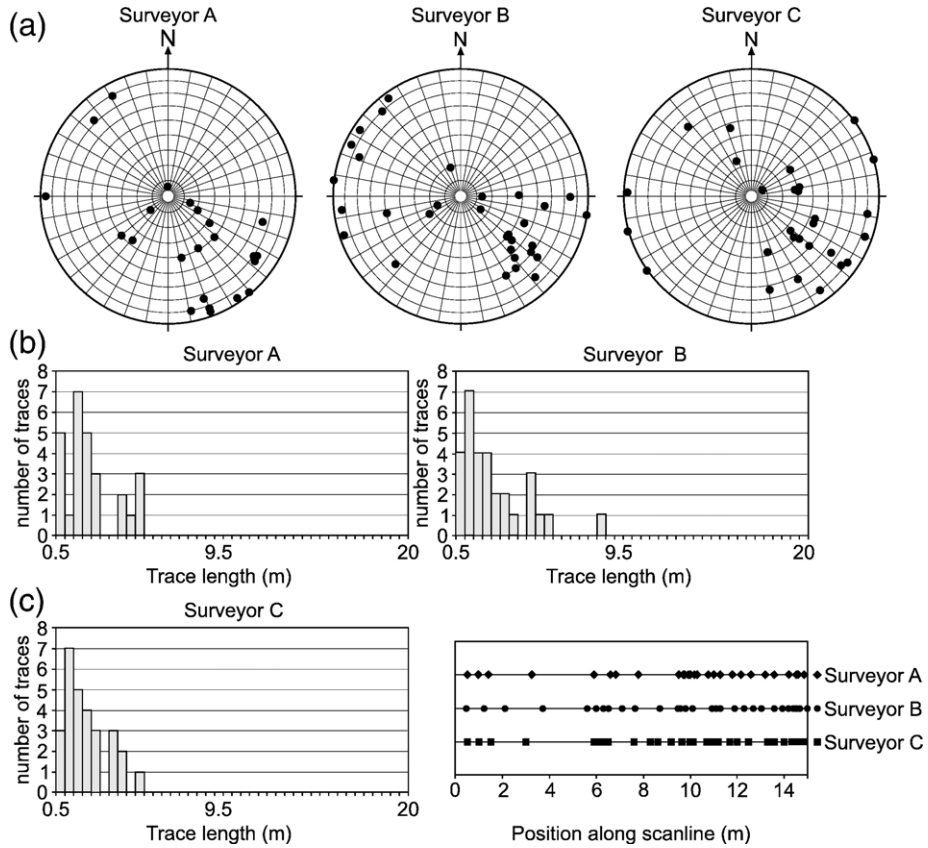

Fig. 3. Comparison of discontinuity data measured by three workers at Habberley Valley, Kidderminster, West Midlands (National Grid Reference SO802 778): (a) discontinuity orientations (upper hemisphere, equal area projection); (b) discontinuity trace lengths; (c) position of discontinuities along the scan line.

faced, 30-edged polyhedron (i.e. a regular icosahedron). This gives 15 uniformly distributed directions.

Advective transport can be simulated in NAPSAC through particle tracking techniques.

4. Field data results

4.1. Scan line survey

Figs. 4 and 5 show plots of orientation and trace length (i.e. length seen in the exposure) for all discontinuities for each site, and Figs. 6 and 7 show the same data combined for all sites together with the proportion of censoring types. Twenty two percent of the total discontinuities recorded were granulation seams. Of the non-granulation seam disconformities, 91% were fractures with unaltered walls or surface staining only; 5% were fractures with slightly altered joint walls with sand fills; and 4% had other fills. Qualitative inspection of Figs. 4 and 5 suggests that the discontinuities at each site have broadly similar characteristics.

Fractures were found almost always to cut through the granulation seams in cases where they met, and hence the granulation seams are not directly relevant to discussion of the fracture network properties, though will clearly affect the interaction of matrix and fracture flow.

4.2. Borehole logs

Data from the borehole CCTV logs are consistent with exponential fracture spacing. No variation with depth is apparent except at one site out of seven: this might be expected as the data set is relatively small and limited to depths less than 150 m below ground level. Fracture frequency appears to be unaffected by formation and lithology as high linear correlation coefficients ($R^2 > 0.85$) are found for five out of seven boreholes when average fracture frequency over a given depth interval for one borehole is plotted against the same parameter for another borehole. The average vertical discontinuity spacing is around 0.39 m.

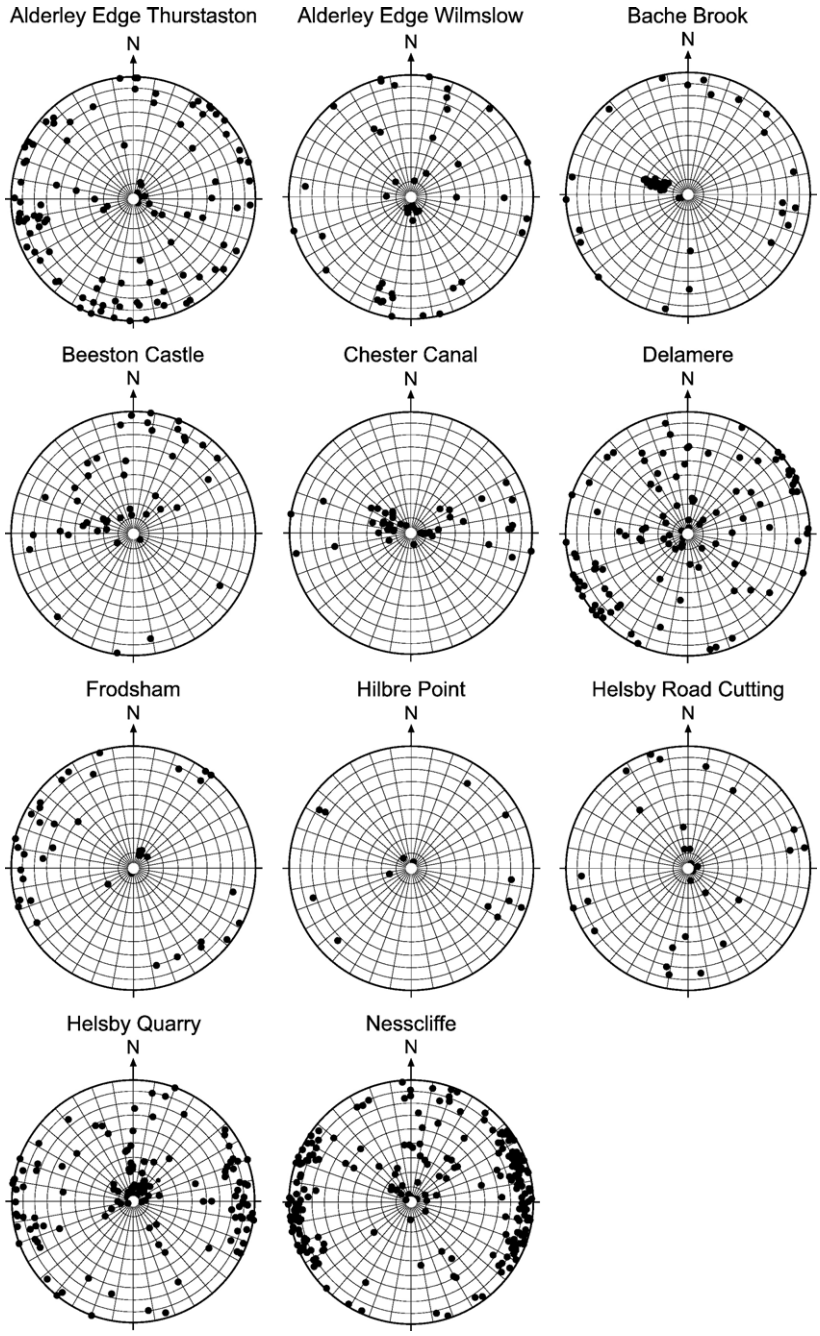

Fig. 4. Stereoplots from scan line survey locations (upper hemisphere, equal area).

To assess the proportion of fractures that transmit significant flow, locations of changes in gradient of temperature and conductivity log traces were compared with fracture locations as identified by CCTV logging. The data were grouped into 5 m depth intervals: if a change in gradient in the 5 m interval occurred, at least one fracture and at most all of the fractures in the interval were assumed to have significant flow. A summary of the resulting data set is shown in Table 3, and indicates that around 9% of the discontinuities intersected by the boreholes have significant flow, with lower and upper bounds of 4.5 and 10.7%. These figures are likely to be underestimates as they depend on the detection limits of the logging method and on the presence of

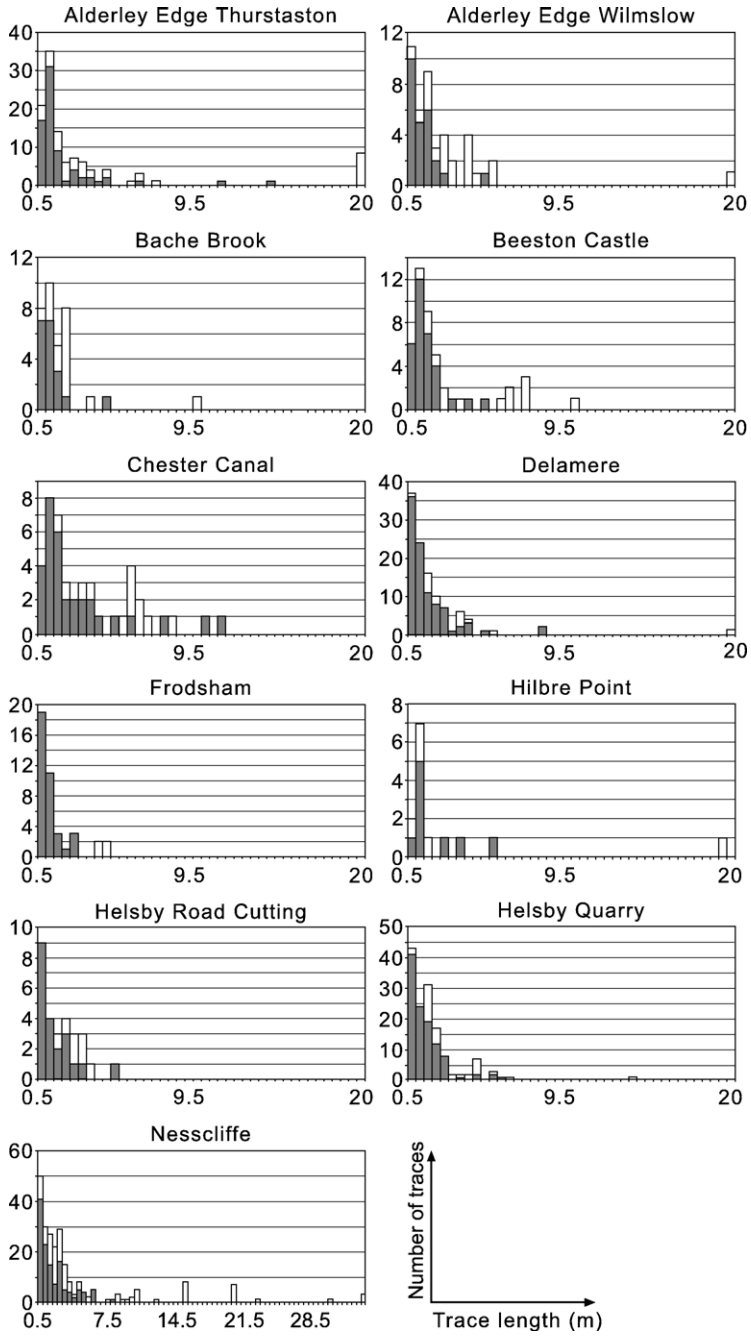

Fig. 5. Trace length histograms for each survey site. Un-shaded bars indicate fracture traces censored by the edge of the outcrop.

thermal or conductivity variations. Morin et al. (1997), also using logging evidence, suggested that around 18% of the discontinuities in the Triassic Passaic Formation of New Jersey, USA, were associated with significant flows. Of the 1054 fractures mapped by Bouch et al. (2006) from core from boreholes in the Triassic Sandstone sequence at the University of Birmingham, UK, only 6% could be unambiguously identified as natural, the remainder being interpreted either as drilling induced (53%) or of ambiguous origin. It is not possible to distinguish simply between flows resulting from an interconnected network of discontinuities and those due to drainage of a significant region of the matrix by a single, large discontinuity. Thus, the percentage of flowing

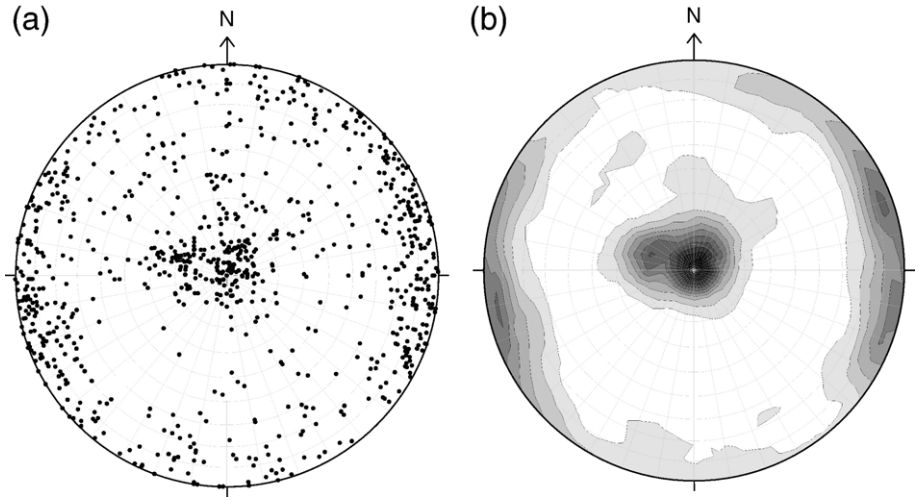

Fig. 6. (a) Stereoplot of scan line data from all survey sites (upper hemisphere, equal angle projection), and (b) shaded density contour plot of the same data (dark colour represents high density).

discontinuities is not a direct measure of the connectedness of discontinuities.

5. A quantitative description of the fracture network

5.1. Definition of fracture sets

A first attempt at definition of discontinuity groupings was made using the orientation data. Fig. 8 indicates four groupings of discontinuities: Group A includes all sub-horizontal fractures; B includes the sub-vertical, north–south striking discontinuities; C includes sub-vertical, east–west striking discontinuities; and D includes all the remaining discontinuities. The grouping boundaries are somewhat arbitrarily defined. All groupings are approximately normally distributed in terms of dip and direction, except for Group A (to assess this, all dips were measured in one direction and dip directions altered accordingly). Kolmogorov–Smirnoff tests of whether each grouping at individual sites was likely to be part of a population formed by data on that grouping obtained from all sites suggested that in most cases the groupings were tenable at the 95% significance level; Group A was least appropriate (Jeffcoat, 2002). Mann–Whitney testing of groupings at each site against the same groupings at each of the other sites again indicated that the groupings are statistically valid at the 95% significance level (Jeffcoat, 2002).

Trace length distributions are approximately exponential, except in the case of Group B. Accordingly, Group B was subdivided into discontinuities greater and less than 10 m long. Censoring data suggested Group A might also be subdivided into two classes: the censored discontinuities (i.e. those which continue beyond the edge of the exposed outcrop) are assumed to be true bedding plane discontinuities, whereas the uncensored discontinuities are often associated with cross-lamination structures.

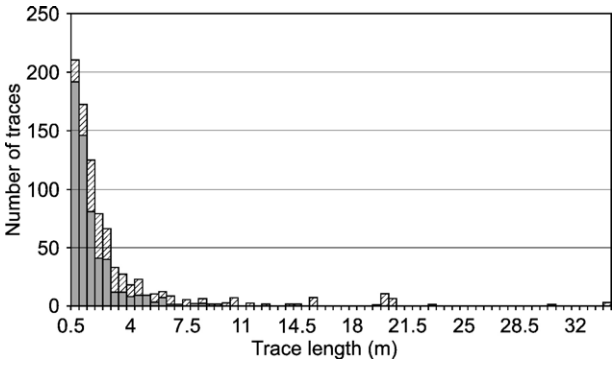

Fig. 7. Histogram of trace lengths from all survey sites. Hatched bars indicate fracture traces censored by the edge of the outcrop.

Table 3
Percentage of discontinuities through which detectable flow occurs

Site	Maximum % flowing	Minimum % flowing	Mean % flowing
Burton	4.5	4.5	4.5
Clockhouse Farm	9.8	9.8	9.8
Saughill Massie	7.8	5.9	6.9
South John St	8.3	5.8	7.0
Manchester Road	9.7	7.2	8.4
Vauxhall Road	12.4	8.9	10.7
Haskayne	9.6	8.2	8.9
All sites			8.9

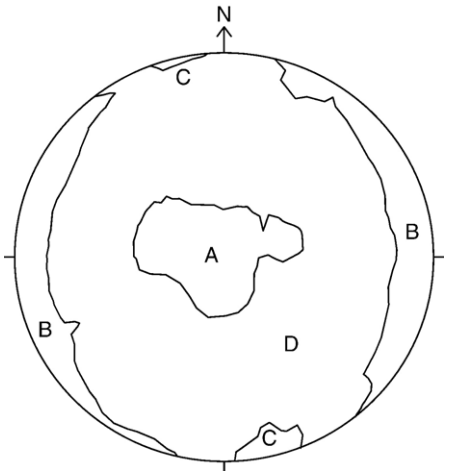

Fig. 8. Initial groupings of discontinuities (A, B, C, and D) from scan line survey data.

Thus, finally, six sets were defined. Group A was divided into Set 1, horizontal large bedding plane fractures, and Set 5, sub-horizontal short discontinuities. Group B was partitioned into Set 2, short (<10 m) sub-vertical north–south striking discontinuities, and Set 6, long (>10 m), sub-vertical north–south striking discontinuities. Set 3 was identified with Group C, sub-vertical east–west striking discontinuities, and Set 4 with Group D, randomly orientated discontinuities not included in other sets.

The validity of this classification is further supported by the consistency of the parameter values for each set, as discussed below.

5.2. Properties of each set

5.2.1. Length distributions

To generate stochastic fracture networks, NAPSAC requires statistical distributions representing the three-dimensional properties of the fractures. These include fracture length, width, dip, strike and orientation within the fracture plane. These distributions have to be inferred from the results of the scan line surveys, taking into account biases created by the truncation and censoring of discontinuity traces. Fig. 9 shows the distribution of trace lengths in each set for all sites.

Set 1 discontinuities are all censored by the exposure size, and are assumed to extend fully across the modelled domain in all calculations.

The issue of censoring by the visible boundaries of the outcrops was addressed where possible using the method of Laslett (1982). This method uses a likelihood function

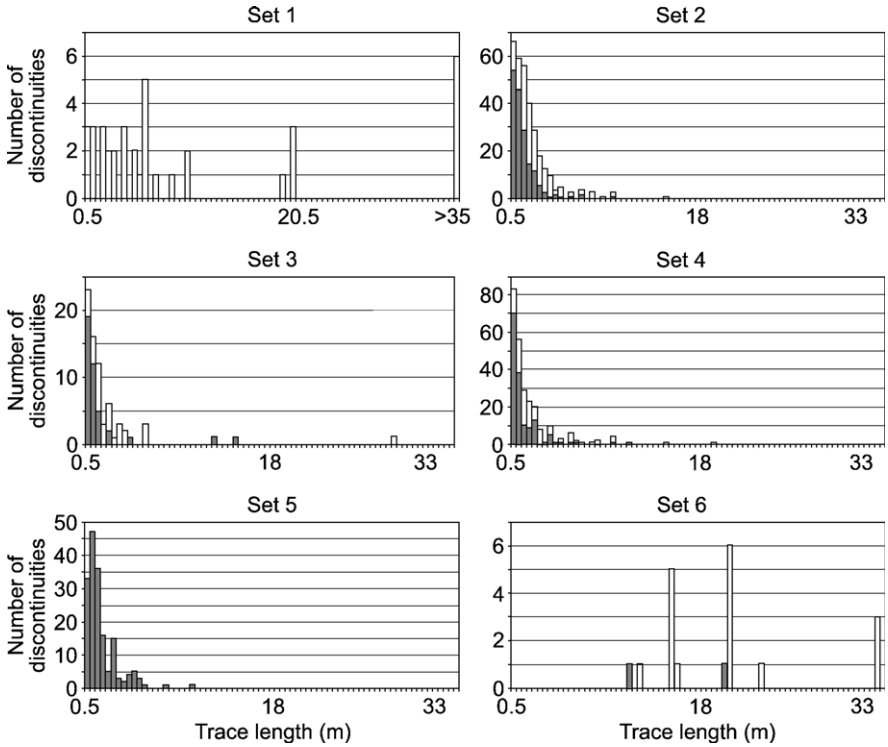

Fig. 9. Distribution of trace lengths in each set for all survey sites. Un-shaded bars indicate fracture traces censored by the edge of the outcrop.

which expresses the probability that the set of observed (and possibly censored) trace lengths represent samples drawn from an underlying statistical distribution of uncensored lengths of a given form, characterised completely a given parameter or set of parameters. Given that the form of the underlying distribution is known, its optimum parameter value or set of values can be determined by maximising the likelihood function. Warburton (1980) gives expressions for the pdf and cdf of the required, underlying length distribution for traces produced by the intersection of parallelogram-shaped discontinuities of constant aspect ratio with a planar outcrop, as observed using a scan line survey, which also accounts for truncation bias. The discontinuities are described by parameters characterising their dip, strike, orientation, and aspect ratio (which are all assumed to be constant) and the pdf of their length, $f(x)$. In the absence of evidence to the contrary, all discontinuities were assumed to be square and orientated with one edge horizontal. For Sets 2, 3, 4 and 5 the distribution of discontinuity lengths was assumed to be exponential with pdf given by

$$f(x) = \lambda \exp(-\lambda x)$$

and hence described by a single parameter, λ. For Sets 2 and 3 the Laslett likelihood function was derived analytically as a function of λ by substituting the above value of $f(x)$ into the Warburton expressions and then substituting these into the Laslett's expression for the likelihood function. The derivation is largely elementary but quite lengthy and so is not reproduced here. The likelihood function is then maximised numerically to give the optimum value of λ (Jeffcoat, 2002). The derived three-dimensional length distributions were validated by using NAPSAC to predict scan line survey data sets. The parameter, λ, was calculated for each set and globally for each site. The simulated cdfs were compared with the observed ones visually and using the Kolmogorov–Smirnoff test (Jeffcoat, 2002). It was concluded that the global parameters provided an adequate classification for most sets of field data. The final parameters are listed in Table 4.

Sets 4 and 5 consist of discontinuities with a wide range of orientations, and no appropriate direct method could be found to enable estimation of the parent distribution. Accordingly, an empirical approach was adopted using NAPSAC: for each outcrop with substantial field data, a large number of discontinuities were simulated in a window the shape of the outcrop and the exponential distribution parameter varied systematically until a good fit to the appropriate trace length cdf from field scan line data was obtained. Goodness of fit to the cdfs was checked visually and by using Kolmogorov–Smirnoff tests (Jeffcoat, 2002). The final λ values chosen were those that provided the best compromise, judged visually, for all the scan lines tested. Discontinuities in Set 4 were uniformly distributed over all orientations except those of the other sets. The final agreement was less good than for Sets 2 and 3. The parameters are given in Table 4.

Ignoring granulation seams, there are only 20 observations of fractures in Set 6, all of which are censored, and hence Set 6 fractures were assumed to cross the entire model domain in all calculations.

5.2.2. Density

The linear density (the number of discontinuities per unit length, P_{10}) was calculated for each set at each site with the appropriate correction made for orientation bias. Volumetric density (the number of discontinuities per unit volume, P_{30}) was then calculated from

$$P_{30} = P_{10}/A$$

where A is the average area of the discontinuities (e.g. Herbert, 1992). For square discontinuities with exponentially distributed side lengths, the average area is twice the square of the mean length. That is

$$A = 2/\lambda^2.$$

For the sub-horizontal Sets 1 and 5, scan line survey data indicate rather greater frequencies than borehole CCTV surveys. As borehole data were considered more reliable because the survey direction is $\sim 90°$ to the fractures, discontinuity frequency data from the scan line surveys were modified by simple proportioning to reflect the properties seen in the borehole data.

For Set 4, the "random" orientation set, the approach described above cannot be applied. Hence, the trial-and-error NAPSAC approach as used to estimate Set 4 length distributions was again employed.

All results were checked by generating the discontinuity sets using NAPSAC and comparing with the field data. The densities of the different fracture sets showed different ranges of variation from site to site, with Sets 2 and 3 displaying greater variability than Set 4, for example. No attempt was made to reproduce this variability, the aim being simply to confirm that the representative density chosen was reasonable: the subsequent modelling work (see below) included investigation of the network with both these set densities and with individual set densities equal to zero. The derived densities are listed in Table 4.

Table 4
Properties of the discontinuity and fracture sets

Set			1	2	3	4	5	6
1. Description (% granulation seams)			Long bedding planes (0)	Short N–S sub-vertical (43)	E–W sub-vertical (26)	Random (23)	Short bedding planes (0)	Long N–S sub-vertical (90)
2. Orientation	Dip direction	Mean	90	265	351	270	292	274
		Spread	0	29	14	±180	71	30
		Distribution	normal	normal	normal	uniform	normal	normal
	Dip	Mean	3	89	85	45	2	89
		Spread	0	8	10	±45	15	90
		Distribution	Normal	Normal	Normal	Uniform	Normal	Normal
3. Length (m)		Mean ($1/\lambda$)	>NAPSAC generation width	0.574	0.3	0.55	0.3	>NAPSAC generation height
		Spread	N/a	N/a	N/a	N/a	N/a	N/a
		Distribution	Uniform	Exponential	Exponential	Exponential	Exponential	Uniform
4. Transmissivity		μ	−11.56	−11.56	−11.56	−11.56	−11.56	−11.56
(original data in m^2/s)		σ	1.96	1.96	1.96	1.96	1.96	1.96
		Distribution	Log-normal	Log-normal	Log-normal	Log-normal	Log-normal	Log-normal
5a. Density of discontinuities (m^{-3}) [separation, m]			(Generation length/mean spacing)/ NAPSAC generation volume	0.437 [3.5]	0.005 [~1 km]	1.22 [1.35]	12.9 [0.43]	1/(14.29 × mean plane area)
5b Density of fractures (i.e. density of all discontinuities except granulation seams) (m^{-3}) [separation, m]			(Generation length/4.61m)/NAPSAC generation volume	0.25 [6.1]	3.7×10^{-3} [~1.5 km]	0.94 [1.76]	12.9 [0.43]	Negligible

5.2.3. Transmissivity

Fracture transmissivity was estimated by comparing hydraulic conductivity values measured in the field with those measured in the laboratory. Packer test data were obtained from Brassington and Walthall (1985) for three boreholes in the north of the Cheshire Basin. Laboratory data were obtained from Campbell (1982) for the same boreholes. This approach assumes differences in scales of measurement between field tests (a few metres) and laboratory tests (a few centimetres) are unimportant. In addition, during the packer testing, some measured intervals may be intercepted by unconnected fractures which will nevertheless increase the apparent packer test permeability values, thus leading to an overestimate of rock mass permeability and therefore also of fracture transmissivity. The sensitivity of the final model results to the estimated fracture transmissivity is discussed in detail in a later section.

Fracture occurrence in the boreholes was estimated from CCTV log data interpretations given in unpublished North West Water Authority (NWWA) investigation reports (summarised in University of Birmingham and NWWA, 1981). The geometric means of the laboratory-measured matrix hydraulic conductivity for the three boreholes were 1.7×10^{-6} ms^{-1}, 1.9×10^{-6} ms^{-1}, and 5.8×10^{-6} ms^{-1}. Borehole-averaged matrix permeability values were used as they gave very similar results to interval-specific matrix permeability values and avoided problems in the intervals where laboratory data were not available.

Fracture transmissivity was assumed to be log-normally distributed, and so the pdf of discontinuity transmissivity, i.e. including closed fractures and granulation seams, could be expressed in the form:

$$f(T;\mu,\sigma)=\begin{cases}\dfrac{p}{\Delta T} & \text{if } T<\Delta T\\ \dfrac{1-p}{\sigma\sqrt{2\pi}}\dfrac{1}{T}\exp\left[-\dfrac{(\ln T-\mu)^2}{2\sigma^2}\right] & \text{if } T\geq\Delta T\end{cases}$$

where

ΔT	is an arbitrarily small value of transmissivity, T
p	is the proportion of non-flowing discontinuities
μ	is the mean of ln$T$
σ	is the standard deviation of ln$T$

Estimates of the log-normal parameters, μ and σ, and the proportion of non-flowing discontinuities, p, were then obtained numerically using a maximum likelihood method modified from Herbert (1992). For this calculation, it is assumed that discontinuity transmissivities are independent and hence additive within a packered interval (and also that the matrix and fracture transmissivities are additive, as implied above). First, the total discontinuity transmissivity of a packered interval is taken to be the transmissivity measured in the field minus the matrix transmissivity for the interval estimated from laboratory tests on cores. Where this leads to a negative value, the total discontinuity transmissivity is assumed to be zero. These values are then used in the log likelihood, which is given by

$$L=\sum_{j=1}^{N}\log f_{n_j}(T_j)$$

where

T_j	is the total discontinuity transmissivity of the jth packered interval
f_{n_j}	is the pdf of the sum of the n discontinuities in the jth packered interval

The log likelihood is then maximised using a numerical optimisation routine. The calculation requires the determination of f_{n_j} which is evaluated numerically from

$$f_{n_j}=\int_0^T f_{(n-1)_j}(T-\tau)f(\tau)d\tau$$

(Herbert, 1992). These calculations were done for each borehole individually and for all three boreholes simultaneously.

Because the packer test data are affected principally by sub-horizontal fractures, and no other suitable data exist, all discontinuity sets were assigned the same transmissivity distribution parameters ($\mu=-11.56$, $\sigma=1.91$, original data in m^{2}s^{-1}), giving a mean transmissivity of 5.91×10^{-5} m^{2}s^{-1} (equivalent to an hydraulic aperture of approximately 400 μm). The proportion of flowing fractures was found to be 73%. This appears to contradict the results of the borehole logging undertaken during this study, which suggested 9% of fractures to have significant flow. However, the number of fractures recorded from CCTV logs during the current investigation was around 7.5 times greater than recorded during the NWWA investigations (see above, this section), and hence the absolute number of flowing fractures is in fact very similar (e.g. 24 expected in a 100 m section from the logging in this study, 26 from the NWWA data sets). It was assumed that all Set 1 fractures are flowing, and that enough Set 5 fractures are flowing so that the total proportion of Sets 1 and 5 flowing amounts to 9%. This was represented in the data sets by scaling the density of the discontinuities: Set 1 mean

spacing therefore remained unchanged at 4.6 m, and Set 5 density was changed from 12.9 m^{-3} to 0.25 m^{-3}. All the discontinuities in the other sets, in the absence of specific data, were assumed to be flowing.

5.2.4. Fill

Most discontinuities appear to be unfilled with unaltered walls, though granulation seams also comprise a significant proportion of total discontinuities. In Set 6, 90% of discontinuities are granulation seams, leaving only 20 fractures in the Set. Accordingly, Set 6 was ignored in the fracture network description, though some exploration of its effect has been undertaken using NAPSAC (see below). In the other sets, granulation seams make up to about 40% of discontinuities, and hence all densities were scaled to take this into account (Table 4). Other types of fill have been accounted for implicitly in the adjustments already made in the previous section.

6. Determination of the properties of the fracture network

6.1. Introduction

The properties of the fracture (i.e. non-granulation seam) network, as represented in Table 4, were investigated using NAPSAC. Intergranular flow is not considered and, because non-granulation seam discontinuities are so rare in Set 6, this set is not included in the initial simulations. All fractures are assigned the same transmissivity distribution (see Section 5.2.3) unless otherwise indicated. The aims of the investigation were to determine: minimum representative volumes (MRVs) for hydraulic conductivity; effective hydraulic conductivity tensors; the role of different fracture sets; and tortuosity. Extensive initial experimentation indicated that, for a cubic volume of sandstone with the fracture network described in Table 4, a fracture generation region extending 3 m beyond the solution region in all directions is required to reduce edge effects on simulated fracture density to an acceptable level, and that the maximum solution region for a practicable run time is a cube of side 35–40 m. The effective hydraulic conductivity tensor was obtained in NAPSAC by successively applying steady state hydraulic gradients across the cube in 15 uniformly distributed orientations, solving for the flow through the fracture network for each set of boundary conditions, and numerically determining the tensor that best simultaneously predicts the bulk flows across each of the faces of the cube (see above).

6.2. The minimum representative volume for hydraulic conductivity

Fig. 10 shows how the mean, and upper and lower quartiles of the components of the hydraulic conductivity tensor for the fracture network of Table 4 change as a function of size of the cube of rock investigated. At each cube size, 50 simulations were run. The MRV appears to be close to a 35 m cube.

The mean and standard deviations of the components of the effective hydraulic conductivity tensor for a 35 m cube are given in Table 5. The mean values represent the best estimate upscaled hydraulic conductivity and form a base case for further investigations. The conductivity tensor can also be expressed in terms of the magnitudes and directions of the principal components, $\overline{K}_{max}$, $\overline{K}_{inter}$ and $\overline{K}_{min}$ (Table 6). Flow is dominated by the sub-horizontal fractures, especially those of Set 1. This leads effectively to isotropy in a plane that dips at between 2° and 3° to the east. The anisotropy ratio of 1.007 in this plane ($\overline{K}_{max}$:$\overline{K}_{inter}$) is insignificant. At right angles to the plane, the hydraulic conductivity, $\overline{K}_{min}$, is approximately 23 times smaller. Thus, the effective hydraulic conductivity can be visualised as an oblate spheroid.

The modelling has assumed that the Set 1 fractures cut the whole of the modelled region. This suggests the existence of another larger MRV at a scale greater than the size of Set 1 fractures. As Set 1 fractures are bedding plane fractures, it is possible that their size will be controlled by the lateral extent of individual beds. Excluding mudstones, which may be associated with less permeable bedding plane discontinuities, individual beds are likely to have lateral extents of less than a few tens of metres; however the only hard evidence from the fracture survey is that these features are more extensive than the outcrops surveyed. Set 6 may also be associated with the larger scale MRV: Set 6 fractures may represent faults, and as such may be up to kilometres in length.

6.3. Sensitivity of the hydraulic conductivity tensor to the fracture transmissivity distribution

Since the estimation of the distribution of fracture transmissivity from field and laboratory tests is an uncertain process, the sensitivity of the upscaled hydraulic conductivity tensor to the fracture transmissivity distribution was investigated by varying the mean and standard deviation of the natural logs of the transmissivity (μ and σ) about their base case values of −11.56 and 1.91 respectively. In each case the same fracture geometry was examined, namely that which gave the

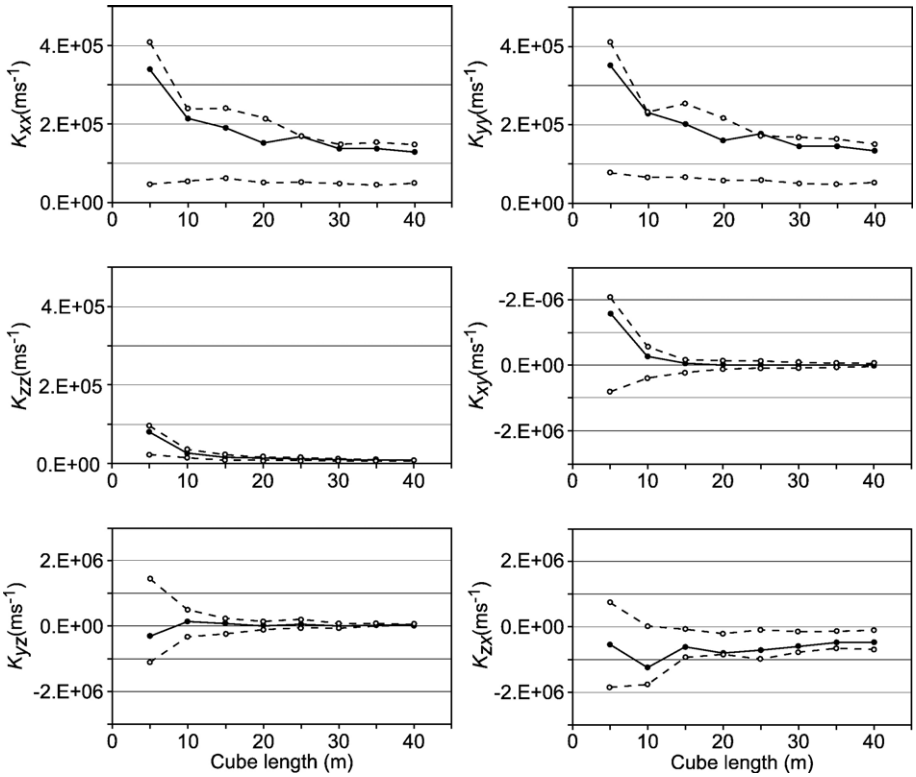

Fig. 10. The mean (solid line), and upper and lower quartiles (dashed lines) of the components of the hydraulic conductivity tensor for the fracture network of Table 4 as a function of size of the cube of rock investigated.

tensor closest to the average tensor during the MRV experiments.

Sensitivity of the upscaled tensor to σ was tested by keeping μ constant at -11.56, and varying σ between zero and 3.3. With σ equal to zero, all fractures have a transmissivity of 1.0×10^{-5} m^{2}s^{-1}. The upper value of σ was chosen so that the resulting mean transmissivity [given by $\exp(\mu+\sigma^2/2)$] was equal to the ninetieth percentile in the observed distribution (2.2×10^{-3} m^{2}s^{-1}).

For the μ sensitivity analysis, σ was held constant at 1.91 and μ was varied in the interval -11.56 ± 3.62, which corresponds to mean transmissivities ranging between 1.6×10^{-5} m^{2}s^{-1} and 2.2×10^{-3} m^{2}s^{-1}.

The results for the extreme values of μ and σ are given in Table 7, expressed in terms of anisotropy ratios and the ratio between the calculated K_{max} and $\overline{K}_{max}$ (values in Table 6). Between these extremes, the upscaled tensor varies smoothly. The effect of varying μ is straightforward: the directions of the principal tensor components remain unchanged, but their magnitudes are scaled leaving anisotropy ratios unaltered. This follows from the fact that the ratio of the mean to the standard deviation of the fracture transmissivity is independent of μ.

Compared with the results of varying μ, changing σ produces a less dramatic effect on K_{max}. However, changes do occur in the anisotropy ratios and there is a small, but noticeable, effect on principal component directions. Large values of σ retain isotropy in the $K_{max}-K_{inter}$ plane, leaving its dip unchanged, whereas the smallest value increases anisotropy in the plane and its dip from 3° to 9° to the east.

Table 5
Mean and standard deviation of the components of the effective hydraulic conductivity tensor

	K_{xx}	K_{xy}	K_{xz}	K_{yy}	K_{yz}	K_{zz}
Mean (ms^{-1})	1.4×10^{-5}	-7.2×10^{-9}	-5.1×10^{-7}	1.4×10^{-5}	1.6×10^{-9}	6.3×10^{-7}
SD (ms^{-1})	1.5×10^{-5}	1.6×10^{-7}	5.3×10^{-7}	1.5×10^{-5}	1.0×10^{-7}	4.4×10^{-7}

Table 6
Magnitude and direction of the principal components of mean effective hydraulic conductivity, $\bar{K}_{max}$, $\bar{K}_{inter}$ and $\bar{K}_{min}$

	$\bar{K}_{max}$	$\bar{K}_{inter}$	$\bar{K}_{min}$
Magnitude (ms^{-1})	1.4×10^{-5}	1.4×10^{-5}	6.1×10^{-7}
Direction unit vector	$\begin{bmatrix}-9.48\times10^{-1}\\3.15\times10^{-1}\\3.62\times10^{-2}\end{bmatrix}$	$\begin{bmatrix}3.15\times10^{-1}\\9.49\times10^{-1}\\-1.19\times10^{-2}\end{bmatrix}$	$\begin{bmatrix}-3.80\times10^{-2}\\9.89\times10^{-5}\\-9.99\times10^{-1}\end{bmatrix}$

6.4. The influence of fracture Sets 1 to 5 on the upscaled hydraulic conductivity

A set of sensitivity studies was conducted to assess the influence that each of the fracture Sets 1 to 5 has on the upscaled hydraulic conductivity: Set 6 fractures, the long sub-vertical north–south striking ones, are considered separately (Section 6.5). In this investigation, μ and σ were varied over the same range of values as in Section 6.3, but for one fracture set at a time.

The principal results are presented in Table 8. The magnitude of the sub-horizontal components of conductivity is dominated by Set 1, the sub-horizontal bedding plane fractures. This set is also important for vertical flow. Using μ_{max} in place of μ in Set 1 increases K_{zz} by a factor of about 2.4 indicating that Set 1 enhances vertical conductivity by connecting sub-vertical fractures.

Set 4 ('randomly' oriented fractures) and, to a more limited extent, Set 2 (short north–south vertical) have an important effect on the horizontal to vertical anisotropy ratio, but Sets 3 (east–west vertical) and 5 (short horizontal) have little influence on the upscaled conductivity.

Thus, to characterise the system at scales greater than the MRV, much information is required on Sets 1 and 4 (the long bedding plane fractures and random fractures), and little is needed for Sets 5 and 3 (the short bedding plane fractures and the east–west sub-vertical fractures).

6.5. The influence of fracture Set 6 on the upscaled hydraulic conductivity

Set 6 (long north–south sub-vertical fractures), which was excluded from the determination of the MRV, is rare but potentially important. To investigate its impact, one Set 6 fracture was introduced into the MRV cube, and its transmissivity varied from the base case mean, 5.91×10^{-5} m^2s^{-1}, to the largest mean used in the previous sensitivity investigations, 2.20×10^{-3} m^2s^{-1}.

The effect on K_{xx} was insignificant as Set 1 dominates and requires no vertical connections to facilitate horizontal conductivity in the x-direction. The effect on all other tensor components is linear, with the largest effects on K_{zz} and K_{yy}. The consequent effects on anisotropy ratios are summarised in Table 9. The inclusion of a single Set 6 fracture with the lowest transmissivity simulated increases the anisotropy between the larger principal components from one to 1.6, but reduces the ratio between these and the minimum component. In this case, K_{max} has an approximately north–south trend and K_{inter} is east–west.

As the transmissivity of the Set 6 fracture increases, K_{min} and K_{inter} attain the same magnitude, beyond which point K_{inter} becomes sub-vertical and the dip of the plane containing the major principal components increases sharply. The dip direction remains constant at about 7° south of east. Increasing the transmissivity also increases K_{max} significantly. Hence, a Set 6 fracture, if present, makes a significant difference to the properties of the network.

6.6. The influence of the relative flow in fracture Sets 1 and 5 on the upscaled hydraulic conductivity

A major assumption in the development of the conceptual model of fracturing is that all the large bedding plane discontinuities (Set 1) are transmissive fractures, and consequently that the majority of Set 5 fractures, the short bedding plane fractures, do not flow. Further simulations show that reducing the average number of transmissive fractures in Set 1 by 50% and increasing the number of Set 5 fractures so that the total number of fractures in the combined sets remains at 9% results in a reduction in K_{xx} and K_{yy} by nearly 50% and a reduction in K_{zz} by almost 40%, producing a small change in the horizontal to vertical anisotropy ratio. Reducing the transmissivity of Set 1 to zero, so that all the sub-horizontal transmissive features belong to Set 5,

Table 7
Sensitivity of upscaled hydraulic conductivity tensor to the mean (μ) and standard deviation (σ) of the natural logarithm of transmissivity of all sets

	All sets			
	σ_{min}	σ_{max}	μ_{min}	μ_{max}
K_{max}/K_{min}	17.6	50.8	22.9	23.0
K_{inter}/K_{min}	11.4	50.7	22.9	23.0
K_{max}/K_{inter}	1.5	1.0	1.0	1.0
$K_{max}/\bar{K}_{max}$	0.6	2.4	0.03	32.5

K_{max} is the maximum principal component of the mean effective hydraulic conductivity for system with amended σ or μ; $\bar{K}$ is the maximum principal component of the mean effective hydraulic conductivity for system without amended fracture transmissivity properties (i.e. as in Table 6).

Table 8
Sensitivity of the upscaled hydraulic conductivity tensor to the mean and standard deviation of the natural logarithm of transmissivity of individual sets

	Set 1				Set 2				Set 3				Set 4				Set 5			
	σ_{min}	σ_{max}	μ_{min}	μ_{max}	σ_{min}	σ_{max}	μ_{min}	μ_{max}	σ_{min}	σ_{max}	μ_{min}	μ_{max}	σ_{min}	σ_{max}	μ_{min}	μ_{max}	σ_{min}	σ_{max}	μ_{min}	μ_{max}
K_{max}/K_{min}	14.0	61.7	2.7	793.2	24.1	23.4	39.3	18.5	22.9	22.9	22.9	22.9	26.6	18.9	215.4	3.8	23.1	22.7	23.1	22.7
K_{inter}/K_{min}	13.4	61.6	2.7	789.7	23.9	23.0	38.1	17.3	22.9	22.9	22.9	22.9	26.2	18.5	213.7	3.8	23.1	22.7	23.1	22.7
K_{max}/K_{inter}	1.0	1.0	1.0	1.0	1.0	1.0	1.0	1.1	1.0	1.0	1.0	1.0	1.0	1.0	1.0	1.0	1.0	1.0	1.0	1.0
$K_{max}/\overline{K}_{max}$	0.7	2.3	0.06	31.8	1.0	1.0	1.0	1.1	1.0	1.0	1.0	1.0	1.0	1.1	0.9	1.8	1.0	1.0	1.0	1.0

reduces K_{xx} and K_{yy} greatly, and K_{zz} to about 25% of its base case value. In the absence of transmissive Set 1 fractures, the effective hydraulic conductivity tensor can be visualised as a prolate spheroid whose major axis dips at about 60°, to just east of south, with a K_{max} over 50 times smaller than $\overline{K}_{max}$.

The results highlight the dominant effect of Set 1 on horizontal flow and its important role in facilitating vertical flow. Without Set 1 fractures, and in the likely absence of Set 6, the network is poorly connected, with a much reduced effective hydraulic conductivity in which the horizontal components are no longer dominant.

6.7. Tortuosity

Tortuosity, estimated here by dividing the mean advective path length from a source to a plane orthogonal to the mean flow direction by the distance from the source to the plane, has been investigated in the north–south direction in the network. A hundred thousand particles were used to track solute movement across the standard network (Table 4) under a north–south head gradient. Fifty simulations were undertaken for cubes with sides ranging between 5 m and 40 m. The results are shown in Fig. 11. It appears that the MRV for tortuosity in the north–south direction is around 20 m, and that its value is between 1.65 and 1.7.

The sensitivity of tortuosity to transmissivity has been investigated. When μ is changed in all sets simultaneously, very little change in tortuosity occurs: the change is less than 0.2% for $-15<\mu<-8$. Similarly, changes in the μ values for Sets 2, 3, and 5 individually have very little effect (less than 2%). However, for Set 1, which is aligned parallel to the direction of transport direction, tortuosity decreases by around 20% as μ increases from −15 to −8, and for Set 4 (the 'randomly' oriented fractures) it increases significantly (by about 20%) as μ increases. In both cases, the changes occur because a significant proportion of the flow is diverted though these fractures as they become more transmissive.

Tortuosity is insensitive to changes in σ for individual sets. Similarly, there is little change in tortuosity as σ increases beyond about 2 for all sets simultaneously. The greatest change (less than 3%) is seen when σ is reduced to zero from the standard model value.

Including a single, north–south striking, sub-vertical Set 6 fracture also increases tortuosity, in this case by about 9% and through a large-scale distortion of the flow field rather than by many small-scale disturbances as for Set 4.

If all flow in the sub-horizontal sets passes through Set 5, i.e. there is no flow through the large bedding plane fractures, the tortuosity increases by around 80%; however, if 50% of flow passes through Set 5, the tortuosity is increased by only 5%. Again, the importance of the Set 1 fractures is indicated.

Table 9
Sensitivity of upscaled hydraulic conductivity tensor to the transmissivity of a single fracture from Set 6

	SET 6		
Transmissivity (m^2s^{-1})	5.91×10^{-5}	3.61×10^{-4}	2.20×10^{-3}
K_{max}/K_{min}	9.6	5.9	35.4
K_{inter}/K_{min}	5.8	1.2	6.9
K_{max}/K_{inter}	1.6	5.1	5.1
$K_{max}/\overline{K}_{max}$	1.6	4.8	24.4
Dip of $K_{max}-K_{inter}$ plane	2°	5°	83°

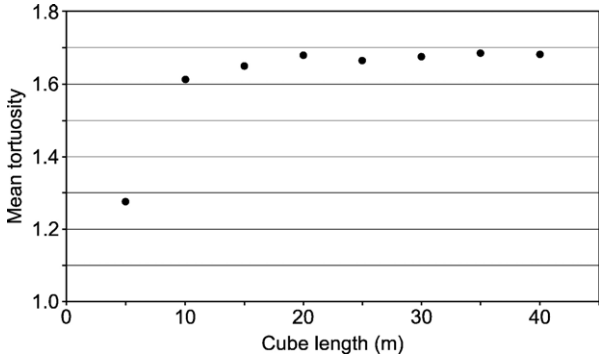

Fig. 11. North–south tortuosity as a function of size of the cube of rock investigated.

7. Discussion and conclusions

This study appears to be the most detailed yet on sandstone fracture networks. Scan line surveys in other UK basins, combined with statistical comparisons suggest that the results might be transferable to most of the English outcrop areas (Jeffcoat, 2002): how relevant the results are to other sandstone sequences is unknown, but presumably similar results will be found in similar sandstones with similar tectonic histories.

Despite much data collection and collation, many assumptions have had to be made in the study, especially in connection with transmissivity, but also with regard to producing adequate statistical distributions of, for example, density, and even simply when comparing results from different methods of survey. The raw data for the well-defined parameters are associated with fairly large errors. Hence, in undertaking the work, much use was made of sensitivity analysis using a discrete fracture network model.

The sandstone fracture network was found to be dominated by large sub-horizontal bedding planes (Set 1) which, given the assumptions made for transmissivity distributions, results in a horizontally isotopic permeability tensor flattened in the *z*-direction. In reality, there are no data on the isotropy of the transmissivities of particular fracture sets. The large bedding planes are also important in increasing vertical permeability, presumably by connecting vertical fractures (members of Sets 2, 3, and 4). If these Set 1 fractures are not present, the network is rather poorly connected. Of the other five sets, Set 4, of "random" orientation, is important in facilitating vertical connections. The only other important set is a rare vertical fracture set, Set 6, which alters the fracture network properties considerably when present. In its absence, the minimum representative volume (MRV) for the permeability tensor for a cubic block appears to be around $35 \times 35 \times 35$ m, but if it is present the MRV may well be much larger. These sizes have implications for hydraulic testing of the aquifer. The tortuosity of the network in the north–south direction is around 1.7, but is much greater in the absence of the large bedding plane fractures. The MRV for the tortuosity, again in a cubic block, is around $20 \times 20 \times 20$ m. From these results it is concluded that in general in order to describe the system, information on three of the six fracture sets present is needed — Sets 1, 4, and 6 (the short bedding plane, east–west sub-vertical, and long north–south fracture sets).

The best-estimate horizontal effective hydraulic conductivity of the network is about 1.2 md^{-1}, which is similar in magnitude to the regional value for the formation (Allen et al., 1997), but the vertical conductivity of the network is 23 times less which is smaller than the vertical bulk conductivity of many individual sandstone beds, but not of a sequence including finer-grained beds. The assumption of random spatial distributions used in NAPSAC's fracture generator will result in few T junctions between vertical and horizontal fractures: this may lead to some underestimation of vertical bulk permeability, but it is unlikely to change the overall anisotropy significantly. The precise effect of different fracture generation techniques (e.g. Swaby and Rawnsley, 1996; Gringarten, 1998; Josnin et al., 2002; Riley, 2004) on the effective hydraulic conductivity remains largely untested.

Possibly the least constrained data set is that relating to the inferred fracture transmissivity distribution. In particular, anisotropy of permeability within the main bedding plane fractures could affect the shape of the hydraulic conductivity tensor profoundly, and hence needs to be investigated. This is not a trivial exercise given the presence of permeable matrix and the size of the MRV. To interpret any field test data it will be necessary to link the network description to matrix flow.

Likewise, any speculation on the implications for solute movement must be tentative given the importance of matrix interactions and the range of possible boundary conditions. However, a few general points on pollutant movement can be made.

For solute movement between boreholes at distances of less than a few tens of metres, sub-horizontal fracturing is likely to be very significant, and this appears to agree with the limited field data (Streetly et al., 2002; Tellam and Barker, 2006).

At larger scales, the relatively high fracture network to matrix conductivity ratio and the low fracture porosity suggest again that enhanced transport might be expected, up to the point where interactions with the matrix attenuate the solute signal. Without further investigation, this distance is unknown. The presence and properties of the Set 1 bedding plane fractures will be crucial. The tortuosity of the network at larger scales appears to be ~ 1.6 (greater in the absence of Set 1).

The combination of Set 1 fractures with the rare Set 6 (large sub-vertical) fractures could mean in unfavourable situations very rapid transport over distances well in excess of the MRV reported here [?e.g. in the case described by Barker et al. (1998)], but only in the ~north–south direction.

Although in the sub-vertical direction the upscaled fracture network conductivities are much less than in the sub-horizontal directions, and less than much of the matrix conductivity, they may nevertheless be important in promoting transport past some of the finer-grained,

more cemented beds in the sandstone sequence. Set 1 fractures are important in maintaining vertical connectivity, so transport will involve sub-horizontal as well as vertical movement.

Granulation seams are common, but field relationships suggest that they will not significantly affect the flow through fractures which intercept them; however, they may focus matrix flows towards these fractures, affecting transport and water/rock interaction. Other types of faulting, probably represented by Set 6 fractures, may show low permeability in directions perpendicular to their planes.

Dense non-aqueous phase liquids may be influenced even more by fractures than dissolved phase pollutants, critically depending on fill within the fractures. Again, lateral movement will be considerably easier than vertical movement, and in some cases, especially where the Set 1 fractures are locally absent, downward migration may be prevented. The total volume of the fractures is relatively small, and hence the fracture network would be expected to fill rapidly, in some cases causing significant driving heads to develop.

Acknowledgements

We would like to thank the UK Natural Environment Research Council for funding Anna Hitchmough (née Jeffcoat), and the Environment Agency, NW Region, and in particular, David Passey and John Ingram, for much support with data and access to boreholes. Bryan Robinson, Ben Furlong, and Alex Bond were all very generous with their help in the field, and Alex is also thanked for help with NAPSAC. Serco Assurance (formerly AEA Technology) is thanked for allowing access to NAPSAC, and Lee Hartley in particular for his support.

References

Allen, A.D., 1969. The Hydrogeology of the Merseyside Area. Unpublished PhD thesis, Department of Geology, University College London.

Allen, D.J., Brewerton, L.J., Coleby, L.M., Gibbs, B.R., Lewis, M.A., Macdonald, A.M., Wagstaff, S.J., Williams, A.T., 1997. The physical properties of major aquifers in England and Wales. British Geological Survey Tech. Report. WD/97/34. Environmental Agency R&D Publication, vol. 8. 312 pp.

Allen, D.J., Bloomfield, J.P., Gibbs, B.R., Wagstaff, S.J., Barker, J.A., Robinson, N., 1998. Fracturing and the hydrogeology of the Permo–Triassic Sandstones in England and Wales. BGS Report No. WD/98/1.

Anon, 1997. The description of rock masses for engineering purposes. Quarterly Journal of Engineering Geology 10, 355–388.

Barker, R.D., Tellam, J.H. (Eds.), 2006. Fluid Flow and Solute Movement in Sandstones: The Onshore UK Permo–Triassic Red Bed Sequence. Special Publication, vol. 263. Geological Society, London.

Barker, A.P., Newton, R., Bottrell, S.H., Tellam, J.H., 1998. Processes affecting groundwater chemistry in a zone of saline intrusion into an urban aquifer. Applied Geochemistry 6, 735–750.

Barnes, R.P., Dee, S.J., Sanderson, D.J., Bowden, R.A., 1998. Interpretation of structural domains in discontinuity data from Nirex deep boreholes at Sellafield. Proceedings of the Yorkshire Geological Society 52 (2), 177–187.

Barton, N.R., 1973. Review of new shear strength criterion for rock joints. Engineering Geology 8, 257–332.

Barton, N.R., Lein, R., Lunde, J., 1974. Engineering classification of rock masses for the design of tunnel support. Rock Mechanics 6, 189–236.

Benton, M.J., Cook, E., Turner, P., 2002. Permian and Triassic Red Beds and the Penarth Group of Great Britain. Geological Conservation Review Series, vol. 24. Joint Nature Conservation Committee, Peterborough.

Bouch, J.E., Hough, E., Kemp, S.J., McKervey, J.A., Williams, G.M., Greswell, R.B., 2006. Sedimentary and diagenetic environments of the Wildmoor Sandstone Formation (United Kingdom): implications for groundwater and contaminant transport, and sand production. In: Barker, Tellam (Eds.), Fluid Flow and Solute Movement in Sandstones: The Onshore UK Permo–Triassic Red Bed Sequence. Special Publication, vol. 263. Geological Society, London, pp. 129–158.

Brassington, F.C., Walthall, S., 1985. Field techniques using borehole packers in hydrogeological investigation. Quarterly Journal of Engineering Geology 18, 181–193.

Brereton, N.R., Skinner, A.C., 1974. Groundwater flow characteristics in the Triassic Sandstone in the Fylde area of Lancashire. Water Services 78, 275–279.

Campbell, J.E., 1982. Permeability characteristics of the Permo–Triassic Sandstones of the Lower Mersey Basin. Unpublished MSc thesis, School of Earth Sciences, University of Birmingham, UK.

Chadwick, R.A., 1997. Fault analysis of the Cheshire Basin, NW England. In: Meadows, N.S., Trueblood, S.P., Hardman, M., Cowan, G. (Eds.), Petroleum Geology of the Irish Sea and Adjacent Areas. Special Publication, vol. 124. Geological Society, London, pp. 297–313.

Dietrich, P., Helmig, R., Sauter, M., Hötzl, H., Köngeter, J., Teutsch, G., 2005. Flow and Transport in Fractured Porous Media. Springer, Berlin.

Entec, 1997. A synthesis of Data Used to Assess the Hydraulic Character of the Sherwood Sandstone Group at Sellafield. Nirex Report No. SA/97/064.

Fowles, J., Burley, S., 1994. Textural and permeability characteristics of faulted high porosity sandstones. Marine and Petroleum Geology 11 (5), 608–623.

Gringarten, G., 1998. Fracnet: Stochastic simulation of fractures in layered systems. Computers & Geosciences 24 (8), 729–736.

Gutmanis, J.C., Lanyon, G.W., Wynn, T.J., Watson, C.R., 1998. Fluid flow in faults: a study of fault hydrogeology in Triassic sandstone and Ordovician volcaniclastic rocks at Sellafield, north–west England. Proceedings of the Yorkshire Geological Society 52 (2), 159–175.

Hartley, L.T., 1998. NAPSAC (Release 4.1) Technical Summary Document. AEA Technology Report AEA-D&R-0271.

Hawkins, A.B., McConnell, B.J., 1992. Sensitivity of sandstone strength and deformability to changes in moisture content. Quarterly Journal of Engineering Geology 25, 115–130.

Herbert, A.W., 1992. Groundwater Flow and Transport in Fractured Rock. Unpublished PhD Thesis, University of Bath.

Howard, K.W.F., 1988. Beneficial aspects of sea–water intrusion. Ground Water 25, 398–406.

ISRM (International Society of Rock Mechanics), 1978. Commission on standardization of laboratory and field tests. Q.J. Rock Mech. Min. Sci. & Geomech. Abstr., vol. 15, pp. 319–368.

Jeffcoat, A.M., 2002. Exploring the hydraulic properties of discontinuity geometry in the UK Triassic Sandstones. Unpublished PhD thesis, School of Earth Sciences, University of Birmingham, UK.

Josnin, J.-Y., Jourde, H., Fénart, P., Bidaux, 2002. A three-dimensional model to simulate joint networks in layered rocks. Canadian Journal of Earth Sciences 39, 1443–1455.

Knott, S.D., 1994. Fault zone thickness versus displacement in the Permo–Triassic Sandstones of NE England. Journal of the Geological Society, London 151, 17–25.

Laslett, G.M., 1982. Censoring and edge effects in areal and line transect sampling of rock joint traces. Journal of the International Association for Mathematical Geology 14 (2), 125–140.

Manzochi, T., Ringrose, P.S., Underhill, J.R., 1998. Flow through fault systems in high-porosity sandstones. In: Coward, M.P., Daltaban, T.S., Johnson, H. (Eds.), Structural Geology in Reservoir Characterization. Special Publications, vol. 127. Geological Society, London, pp. 65–82.

Merin, I.S., 1992. Conceptual model of groundwater flow in fractured siltstone based on analysis of rock cores, borehole geophysics and thin sections. Groundwater Monitoring and Remediation 12 (4), 118–125.

Morin, R.H., Carleton, G.B., Poirier, S., 1997. Fractured-aquifer hydrogeology from geophysical logs, the Passaic Formation, New Jersey. Ground Water 35 (2), 328–338.

National Research Council, 2001. Conceptual Models of Flow and Transport in the Fractured Vadose Zone. U.S. National Committee for Rock Mechanics, National Academy Press, Washington, D.C.

Odling, N.E., Roden, J.E., 1997. Contaminant transport in fractured rocks with significant matrix permeability, using natural fracture geometries. Journal of Contaminant Hydrology 27, 263–283.

Plant, J.A., Jones, D.G., Haslem, H.W. (Eds.), 1996. Basin Evolution, Fluid Movement and Mineral Resources in a Permo–Triassic Rift Setting: The Cheshire Basin. BGS Technical Report WP/96/14R. 263 pp.

Price, M., 1982. A study of vertical variation in the permeability of a Permian Sandstone aquifer, using double packer injection testing. Quarterly Journal of Engineering Geology 15 (1), 67.

Riley, M.S., 2004. An algorithm for generating rock fracture patterns: mathematical analysis. Mathematical Geology 36 (6), 683–702.

Robertson, A., 1970. The interpretation of geological factors for use in slope theory. In: Van Rensburg, P.W.J. (Ed.), Planning Open Pit Mines. Balkema, Cape Town, South Africa, pp. 55–71.

Streetly, H.R., Hamilton, A.C.L., Betts, C., Tellam, J.H., Herbert, A.W., 2002. Reconnaissance tracer tests in the Triassic Sandstone aquifer north of Liverpool, UK. Quarterly Journal of Engineering Geology and Hydrogeology 35 (2), 167–178.

Swaby, P.A., Rawnsley, K.D., 1996. An interactive 3D fracture modelling environment. Society of Petroleum Engineers, Tulsa, SPE 36004, Dallas, Texas, pp. 177–187.

Tellam, J.H., Barker, R.D., 2006. Towards prediction of saturated zone pollutant movement in groundwaters in fractured permeable-matrix aquifers: the case of the UK Permo–Triassic Sandstones. In: Barker, R.D, Tellam, J.H. (Eds.), Fluid Flow and Solute Movement in the Fluvial and Aeolian Sandstones of the UK Permo–Triassic Red Bed Sequence. Geological Society Special Publication, vol. 263, pp. 1–48.

University of Birmingham and NWWA (1981) Saline Groundwater Investigation Phase 1 — Lower Mersey Basin, Summary Report. Unpublished report to North West Water Authority.

Walters, M., 1985. The Application of Geophysical Techniques to a Groundwater Resources study of North Merseyside, England. Unpublished PhD thesis, University of Birmingham, UK.

Walthall, S., Campbell, J.E., 1986. The measurement, interpretation and use of Permian values with specific reference to fissured aquifers. Groundwater in Engineering Geology. Geological Society of London Engineering Geology Special Publication, vol. 3, pp. 273–278.

Walthall, S., Ingram, J.A., 1984. The investigation of aquifer parameters using multiple piezometers. Ground Water 22 (1), 25–50.

Warburton, P.M., 1980. A stereological interpretation of joint trace data. International Journal of Rock Mechanics, Mining Sciences & Geomechanical Abstracts 17 (4), 181–190.

Wealthall, G.P., Steele, A., Bloomfield, J.P., Moss, R.H., Lerner, D.N., 2001. Sediment filled fractures in the Permo–Triassic Sandstones of the Cheshire Basin: observations and implications for pollutant transport. Journal of Contaminant Hydrology 50, 41–51.

Yates, P.G.J., 1992. The material strength of sandstones of the Sherwood Sandstone Group of North Staffordshire with reference to microfabric. Quarterly Journal of Engineering Geology 25, 107–113.